Facile hydrothermal synthesis and formation mechanisms of Bi_2Te_3, Sb_2Te_3 and Bi_2Te_3-Sb_2Te_3 nanowires†

Hongqing Feng,[a] Chunyang Wu,[b] Peng Zhang,[a] Jianli Mi*[a] and Mingdong Dong*[c]

[a]*Institute for Advanced Materials, School of Materials Science and Engineering, Jiangsu University, Zhenjiang 212013, China. E-mail: jlmi@ujs.edu.cn*

[b]*Department of Materials Science and Engineering, Zhejiang University, Hangzhou 310027, China*

[c]*Interdisciplinary Nanoscience Center (iNANO), Aarhus University, 8000 Aarhus C, Denmark. E-mail: dong@inano.au.dk*

†Electronic Supplementary Information (ESI) available: SEM images of Te samples prepared under different pH environment, HRTEM images of Te nanowires, XRD patterns of Bi_2Te_3 samples prepared at different reaction times, TEM images of Bi_2Te_3 nanowires washed with DMF, results of Bi_2Te_3 nanowires prepared without EDTA, HRTEM image of Bi_2Te_3-Sb_2Te_3 nanowires, XRD patterns of Bi_2Te_3-Sb_2Te_3 samples prepared at different reaction times.

A facile and scalable glucose-assisted hydrothermal method has been established for the fabrication of Bi_2Te_3, Sb_2Te_3 and Bi_2Te_3-Sb_2Te_3 nanowires in high yield. PH additives, such as HCl and NaOH, play crucial roles for the fabrication of Bi_2Te_3, Sb_2Te_3 and Bi_2Te_3-Sb_2Te_3 nanowires. It is suggested that fine Te nanowires are initially formed and they serve as templates for the fabrication of tellurides nanowires. Bi_2Te_3 nanowires are obtained by a direct one-step hydrothermal synthesis under acidic condition when HCl is used as pH additive. The as-prepared Bi_2Te_3 nanowires have different wire axes that can be parallel or perpendicular to [001] direction. Two different mechanisms, *i.e.*, structural preference growth mechanism and coherent growth

mechanism are suggested for the formation of Bi_2Te_3 nanowires. Single phase of Sb_2Te_3 can not be obtained under acidic condition due to the slow kinetics of the reduction reaction even at elevated reaction temperatures. A two-step synthesis is proposed for the fabrication of Sb_2Te_3 and Bi_2Te_3-Sb_2Te_3 nanowires, where Te nanowires are first formed with HCl additive and Sb_2Te_3 and Bi_2Te_3-Sb_2Te_3 nanowires are then fabricated with NaOH additive. Besides the enhanced phonon scattering and quantum confinement effect, the structure and composition fluctuation in the Bi_2Te_3-Sb_2Te_3 nanowires may further adjust the energy band structure and improve the thermoelectric properties.

Introduction

There have been persistent efforts in improving the thermoelectric figure of merit (zT) by searching new categories of materials,[1] manipulating band structure,[2,3] and using materials with low-dimensional structures.[4] Nanostructuring can result in enhancements in thermoelectric properties, owing to both a high density of states and an increased phonon scattering. There has been tremendous progress towards improving thermoelectric properties by creating nanostructured materials such as quantum dots,[5] superlattice structures,[6] nanowires,[7,8] and nanostructured bulk materials.[9,10]

Semiconductor nanowires, due to their unique structures and properties, are promising candidates for various energy conversion devices.[11] First, the physical and chemical properties are altered for nanowires compared to the bulk counterparts within the confines of the nanowire surfaces. Second, the transportation of electrons, phonons, and photons can be controlled by the one unconstrained dimension, which makes nanowires ideal materials for technological applications. Particularly, it has been predicted by theoretical studies that semiconductor nanowires may exhibit extremely enhanced thermoelectric efficiency due to the quantum confinement and the significant reduction of thermal conductivity.[12] From this point of view, nanowires have been extensively investigated as promising thermoelectric materials. While many experiments have proved the enhancement of thermoelectric performance of nanowires due to the phonon effect,[7,8] the manipulation of the band structure by dimensional confinement of nanowires to improve the thermoelectric properties remains unclear. For example, measurements of individual Bi_2Te_3 nanowires have only shown weak thermoelectric properties compared with bulk Bi_2Te_3.[13-14] Therefore, it remains a challenge to investigate nanowires for the further improvement of thermoelectric performance. Usually, doping is used to adjust the band structure and carrier concentration. However, it is difficult to control the doping in nanomaterials in the chemical synthesis due to the different chemical properties between the doping atoms and matrix atoms. As a result, it is interesting to investigate the fabrication of nanowires for special structures, such heterostructures, which provides another way to adjust the band structure.

Bi_2Te_3 based materials have attracted tremendous interest for their attractive properties in thermoelectrics,[15] phase-change memory switching effects[16] and topological isolators.[17] Most of the synthesized Bi_2Te_3 based nanomaterials come in two dimensional forms such as nanoplates because of their layered crystal structure with rhombohedral symmetry.[18-20] Traditional electrodeposition methods are commonly used to fabricate one-dimensional Bi_2Te_3 nanowires and templates such as anodized alumina are usually required.[21-24] Hydrothermal synthesis is one of the convenient and highly efficient methods for preparation of nanostructured Bi_2Te_3 based materials. A "green" hydrothermal method was proposed to prepare Bi_2Te_3 compound with nanostring-cluster hierarchical nanostructures using alginic acid as the reducing agent.[25] It was found that morphology and size of the Bi_2Te_3 products depend greatly on the NaOH concentration in the precursor solution. Semiconductor heterostructures represent another interesting direction toward nanostructured materials and the synthesis of Bi_2Te_3/Bi and Bi_2S_3/Bi core-shell nanorods has been reported.[26] Herein, a facile self-assembly hydrothermal method is illustrated to directly fabricate Bi_2Te_3 nanowires by controlling the pH conditions. Moreover, a two-step hydrothermal method is demonstrated for the fabrication of Sb_2Te_3 and Bi_2Te_3-Sb_2Te_3 nanowires. Glucose is used as reducing agent instead of any other toxic reducing agents such as hydrazine, $NaBH_4$, or dimethylformamide (DMF), and the method can therefore be considered to meet the "green" synthesis strategy.

Experimental

All the chemical reagents used in the experiments were analytical grade. The precursors $BiCl_3$, $SbCl_3$ and K_2TeO_3 were used as reactants. Ehylenediamine-tetra-acetic acid sodium (EDTA) and glucose were used as complexant and reductant, respectively. HCl or NaOH was used as pH control additive.

For a typical synthesis of Bi_2Te_3 nanowires, 0.5 mmol EDTA was first dissolved with 12 ml distilled water in a Teflon-lined, stainless-steel autoclave of 18 ml capacity. 0.25 mmol $BiCl_3$ and 0.375 mmol K_2TeO_3 were then mixed with 0.4 g glucose in the above solution. Finally, HCl was added to get the target HCl concentration of about 0.2 M. The autoclave was sealed and heated to the reaction temperature of 180 °C and maintained for 24 h. After the reaction, the autoclave was cooled in air to room temperature. The black products were collected and washed repeatedly with distilled water and absolute ethanol by centrifugation.

To understand the formation mechanism of Bi_2Te_3 nanowires, separate experiments for the synthesis of Te powders with different morphologies, i.e., nanowires and large rods, were performed by changing the pH conditions. For a typical synthesis, 0.375 mmol K_2TeO_3 and 0.4 g glucose were dissolved with 12 ml distilled water in the autoclave. The pH conditions were adjusted to 0.2 M HCl, 0.2 M NaOH, 0.6 M NaOH and without any pH additives, respectively, for each sample. The experiments were performed under 180 °C for 24 h.

For the synthesis of Sb_2Te_3 nanowires, two steps of hydrothermal procedures were performed. In the first step, Te nanowires were synthesized as follows: 0.375 mmol K_2TeO_3 and 0.4 g glucose were dissolved in 12 ml 0.2 M HCl aqueous solution in the autoclave. After heating and maintaining at 150 °C for 12 h, the autoclave was cooled down to room temperature. In the second step, 0.5 mmol EDTA and 0.25 mmol $SbCl_3$ were then added in the autoclave. The pH of the solution was adjusting to basic condition by adding 0.192 g NaOH. The autoclave was heated and maintained at 220 °C for 24 h for the second step synthesis. Similar procedures were conducted for the synthesis of Bi_2Te_3-Sb_2Te_3 nanowires, i.e., after the first step synthesis of Te nanowires, precursors of 0.125 mmol $BiCl_3$ and 0.125 mmol $SbCl_3$ and 0.192 g NaOH were added in the second step synthesis.

The X-ray diffraction (XRD) patterns were measured on a Rigaku D/MAX-2500PC Diffractometer using Cu Kα radiation (λ = 1.5406 Å). The morphology of the products was observed on a JSM-7001F field-emission scanning electron microscope (FESEM). High-resolution transmission electron microscopy (HRTEM) images were obtained using a FEI Tecnai F20 microscope with an accelerating voltage of 200 kV. The chemical compositions were analyzed on the energy-dispersive X-ray spectroscopy (EDX attached to FEI Tecnai F20).

Results and discussion

Fig. 1(a) shows the XRD patterns of the Bi_2Te_3 product prepared by direct one-step hydrothermal route at 180 ºC for 24 h in 0.2 M HCl. The XRD data were corrected for instrumental broadening using a silicon standard and structural Rietveld refinement was performed using FullProf program.[27] There is a good agreement between the calculated and observed patterns, confirming that the product is pure-phase Bi_2Te_3. The calculated unit cell parameters of Bi_2Te_3 product are a = 4.387(1) Å and c = 30.47(1) Å, which are in good agreement with reported data of a = 4.395 Å and c = 30.44 Å.[28] **Fig. 1(b)** and **(c)** are the typical SEM images of different magnifications indicating that Bi_2Te_3 nanowires can be obtained in high yield by the simple hydrothermal method when HCl is used as pH additive. It can be seen from the SEM images that most of the Bi_2Te_3 nanowires have lengths about dozens of micrometers and diameters about 50 nm.

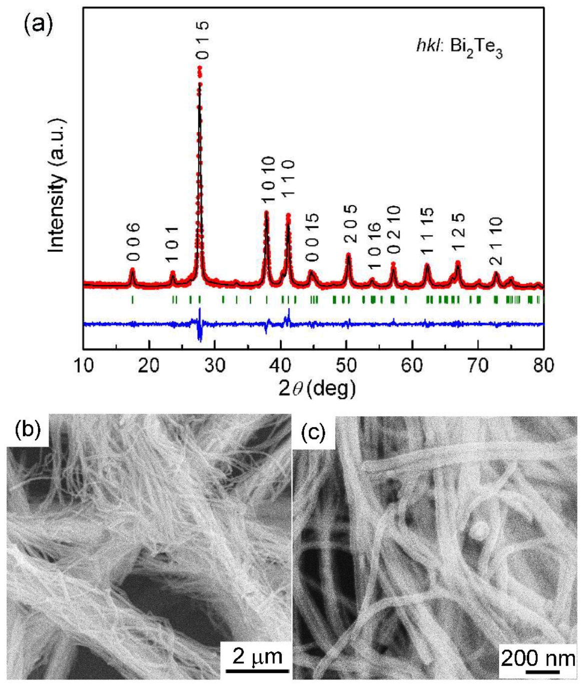

Fig. 1 (a) Observed, calculated and difference XRD patterns of Bi_2Te_3 sample prepared at 180 ºC for 24 h in 0.2 M HCl. (b,c) SEM images of the as-prepared Bi_2Te_3 nanowires.

Bi_2Te_3 based compounds are normally preferred to form in platelets due to its layered crystal structure. Here, it is interesting to see that Bi_2Te_3 nanowires are obtained by the simple hydrothermal synthesis using HCl as pH additive and glucose as reductant. However, only Bi_2Te_3 platelets or particles are obtained if NaOH is used as pH additive instead of HCl, indicating that the pH condition has large effect on the size and morphology of the Bi_2Te_3 products. The results agree well with the previous report that Bi_2Te_3 nanoplatelets or nanoparticles were obtained by hydrothermal synthesis using alginic acid as reductant and NaOH as pH additive.[25] It has been suggested that Te nanorods are the intermediate products and perform as templates for the formation of Bi_2Te_3 nanostructures.[29] Therefore, it can be understood that the size and morphology of intermediate Te products should play crucial roles on the formation of Bi_2Te_3 with different morphologies. For example, tri-wing Bi_2Te_3 nanoribbons were formed using tri-wing Te nanoribbons as templates.[30] To understand the detailed formation mechanisms of Bi_2Te_3 nanowires, different Te samples are prepared under varied pH conditions. **Fig. 2(a)** shows a typical XRD pattern of product prepared under 0.2 M HCl, indicating that pure Te is obtained. Reitveld refinement shows that there is a large disagreement between intensities of the calculated and observed diffraction peaks, which comes from the preferred orientation effects of the XRD data measured on a flat sample holder. The intensity of the observed diffraction peak (110) is much stronger than the calculated one, indicating that the Te sample has a preferred growth direction along *c*-axis. Similar results are obtained for other Te samples except that the diffraction peaks become sharper when the pH changes from acidic to high basic conditions, indicating an increase of crystallite size. **Fig. 2(b)** and **(c)** are the SEM and TEM images of the Te sample prepared under 0.2 M HCl, respectively. It can be seen that fine nanowires with diameters of around 10 to 20 nm are synthesized under acidic condition at 0.2 M HCl. The SEM images of **Fig. S1** show that the diameter of the nanowires increases with no pH additive and 0.2 M NaOH. Large rod-like Te with diameter up to several hundreds of nanometers is obtained when the NaOH concentration is increased to 0.6 M. The HRTEM image of Te nanowire in **Fig. 2(d)** shows that the Te nanowires are single-crystalline. The diffraction fringers with a plane spacing of 0.32 nm are seen, corresponding to the (011) lattice planes in trigonal Te. It indicates that the axis of the Te nanowires is along *c* direction (parallel to [001] direction) according to the crystallographic orientation relationship between the (011) plane and the *c* direction as shown in **Fig. 2(e)**, which agrees with the XRD results. More HRTEM images of Te nanowires can be seen in **Fig. S2**, all of which show that the wire axes are parallel to *c* direction. It has been suggested trigonal Te has a strong tendency to form one dimensional structures along the [001] direction[30] which agrees well with our experiments. The formation of Te nanowires with small diameters under acidic condition can be ascribed to the following reasons. During the reaction, the aldehyde group (–CHO) at one end of glucose molecule is oxidized to carboxylic acid (–COOH). There is alcohol group (–CH_2OH) at the other end of the glucose molecule. Thus an esterification reaction between carboxyl and alcohol group will take place in the presence of the acid catalyst in the present experiments resulting in the formation of organic byproducts of long-chain ester. It can be seen that there are amorphous layers coated on Te nanowires as shown by the TEM image of **Fig. 2(c)**, which could come from the organic residues. The long-chain ester might serve as a template for the synthesis of fine Te nanowires. Furthermore, the presence of organic byproducts introduces an abundance of nucleation sites which is also beneficial for the formation of fine Te nanowires. While under alkaline solution, large Te nanorods are formed without the assistance of organic byproducts. In addition, the reductibility of glucose becomes stronger and the reduction of Te precursor is promoted under alkaline solution because carboxylic acids are produced during the reaction, which may also result in forming larger Te nanorods.

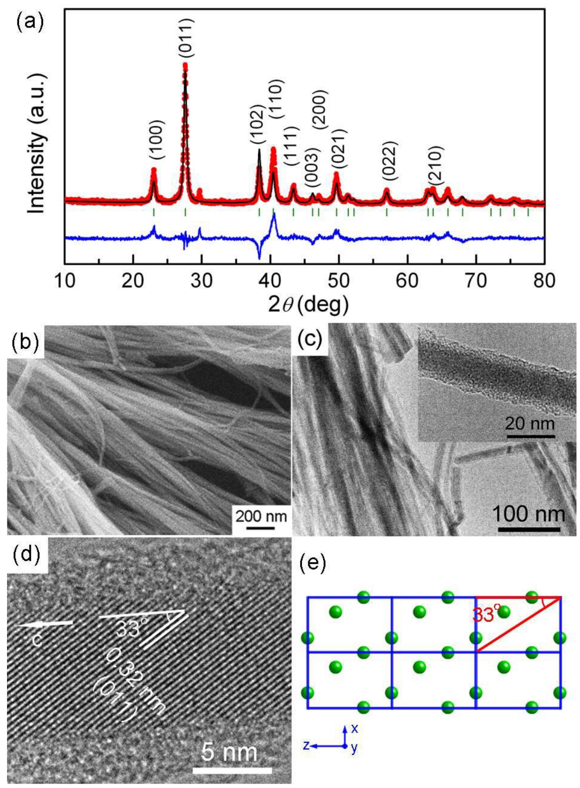

Fig. 2 (a) Rietveld refinement with observed, calculated and difference XRD patterns of Te sample prepared under 0.2 M HCl. (b-d) SEM, TEM and HRTEM images of the as-prepared Te nanowires. (e) Atomic arrangement of trigonal Te in a view direction of [010].

It has been revealed by in situ XRD study that the formation mechanism of Bi_2Te_3 results from the direct reaction between elemental Te and complex Bi ions.[29] The ex situ XRD data (as shown in **Fig. S3**) confirm that Te nanowires are the intermediate products and they act as templates for the formation of Bi_2Te_3 nanowires. As discussed before, it clearly shows that the diameter of one-dimensional Te products is much smaller under acidic condition than that under basic condition. As a result, for the synthesis of Bi_2Te_3 under acidic condition, it is possible to retain the one dimensional morphology because of the short diffusion distance of Bi ions to the Te nanowires attributing to the small diameter of the Te nanowires. For the synthesis in basic conditions, Te nanorods with larger diameters form first as templates. Thus, large microstain is generated during the formation of Bi_2Te_3 due to the mismatch of lattices between Te and Bi_2Te_3, and Bi_2Te_3 tends to grow along its preferred direction perpendicular to the axis of the Te nanowires, contributing to the formation of Bi_2Te_3 nanoparticles or platelets.[25]

Despite of the one dimensional nanostructure of Bi_2Te_3 product, the Rietveld refinement (**Fig. 1**) shows that there is good agreement between intensities of the calculated and observed diffraction peaks (no parameters for preferred orientation are corrected). That is to say, the preferred orientation effect of the XRD data measured on the flat sample holder is negligible for the Bi_2Te_3 nanowires, which is very strange. To interpret this, Bi_2Te_3 nanowires are carefully studied by HRTEM as shown in **Fig. 3**. It can be seen that the as-prepared Bi_2Te_3 nanowires are single-crystalline. However, the nanowires have different wire axes that can be parallel (**Fig. 3(b)**) or perpendicular (**Fig. 3(c)**) to *c* direction. **Fig. 3(d)** shows a Bi_2Te_3 nanowire with a wire axis nearly perpendicular to *c* direction. The detailed atomic arrangement is illustrated in **Fig. 3(e)** with a view direction of [5-51]. The varied wire axes of the nanowires can be a good explanation of the limited preferred orientation effect of the XRD data. It is interesting to see that Bi_2Te_3 nanowires with the different wire axes are obtained, which could be attributed to the different formation mechanisms. In general, the crystal growth rate perpendicular to the *c* axis is much higher than that parallel to the *c* axis for Bi_2Te_3 due to its layered structure with van der Waals bonds between the neighboring Te layers along the *c* axis. Therefore, Bi_2Te_3 nanowires usually tend to grow along [110] direction that perpendicular to the *c* axis. For example, Bi_2Te_3 nanowires with the axis perpendicular to *c* axis were prepared using alumina template by electrodeposition,[21-24,31] and other methods, such as sputtering and vapor-liquid-solid method.[32] However, Bi_2Te_3 nanowires with the axes parallel to the *c* axis are also seen in the present study, which could be attributed to effect of Te templates. Bi_2Te_3 nanowires maintain the same direction as Te templates due to the coherent growth of Bi_2Te_3 and the epitaxial orientation relationship between Bi_2Te_3 nanowires and Te templates are preserved.

It should be also noted that there is a very thick amorphous layer coated on Bi_2Te_3 nanowires as shown in **Fig. 3(a)**. It could be due to that the carboxyl group in chelating agent EDTA was reacted with alcohol group under acidic condition during the synthesis of Bi_2Te_3 nanowires. As shown by the TEM images, the average diameter of Bi_2Te_3 nanowires is below 15 nm, while the whole diameter of the nanowires including the amorphous layer is around 50 nm. The structure of Bi_2Te_3 nanowires coated with a layer of amorphous compounds may have potential special application in microdevices. It is found that the organic layer can be partly removed by washing with DMF as shown in **Fig. S4**. It is found that Bi_2Te_3 nanowires can be also obtained without EDTA under acidic condition indicating the role of surfactant EDTA for directing the special morphology of Bi_2Te_3 is limited in the current synthesis (**Fig. S5**). It also confirms that the fine Te template is a crucial factor for the formation of Bi_2Te_3 nanowires in the present study from the other side.

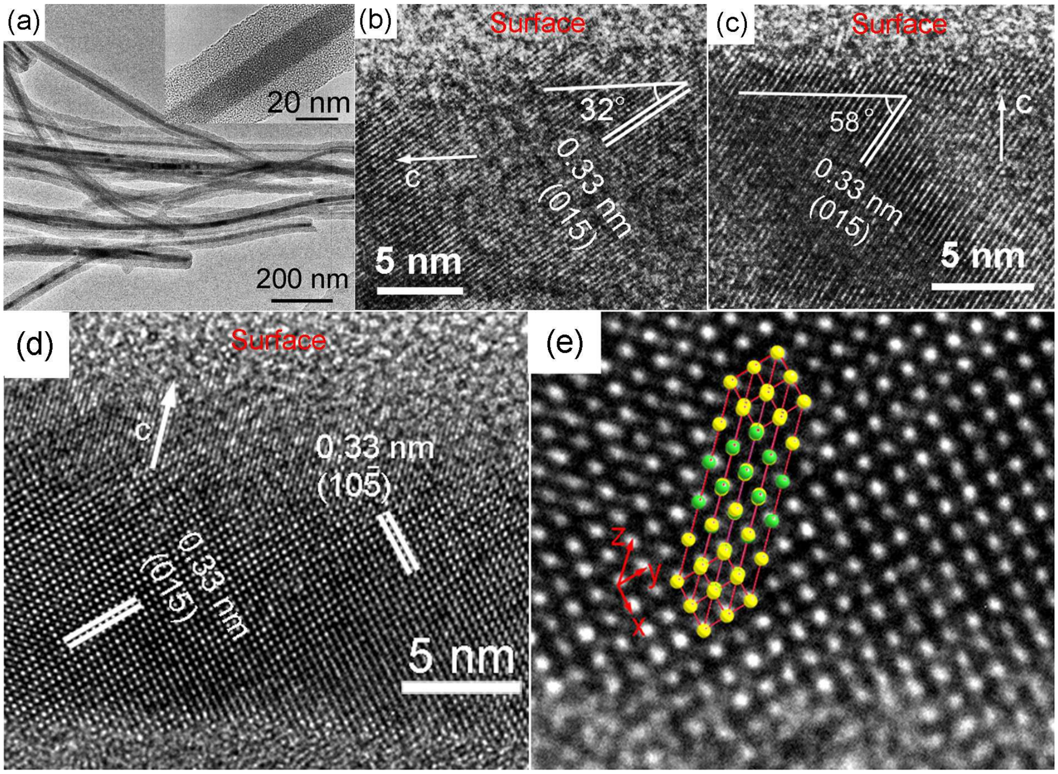

Fig. 3 (a) TEM images of Bi_2Te_3 nanowires prepared at 180 ºC for 24 h in 0.2 M HCl. The inset shows a single nanowire coated with a thick amorphous layer. (b-d) HRTEM images of Bi_2Te_3 nanowire, showing that the Bi_2Te_3 nanowires have different wire axes directions. (e) Part of the HRTEM image of (d) and the detailed atomic arrangement illustrated by 4 unit cells of Bi_2Te_3 with a view direction of [5-51].

Based on the above discussion, two different formation mechanisms are suggested in **Fig. 4**, (i) structural preference growth mechanism resulting in the Bi_2Te_3 nanowires with the wire axes perpendicular to the *c* direction, and (ii) coherent growth mechanism with Te templates leading to the Bi_2Te_3 nanowires with the wire axes parallel to the *c* direction. For both mechanisms, the intermediate product of fine Te nanowires plays an important role in the formation of one dimensional nanostructure of Bi_2Te_3 nanowires. Because of the importance of Bi_2Te_3 in both thermoelectric and topological insulator fields, it could be very meaningful for the fabrication of nanowires with different orientations due to the anisotropic properties of Bi_2Te_3.

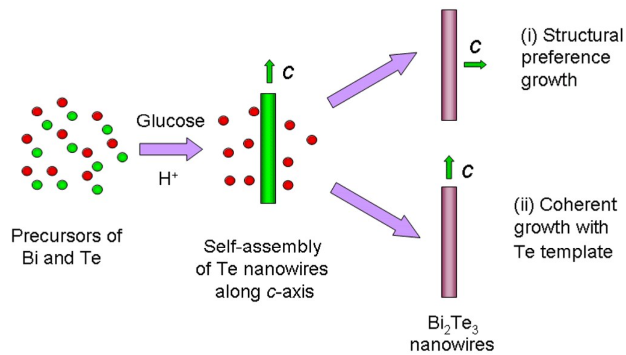

Fig. 4 Schematic illustrations of the two mechanisms for the formation of Bi_2Te_3 nanowires, (i) structural preference growth mechanism, and (ii) coherent growth mechanism.

The anisotropic crystallite size of Bi_2Te_3 nanoplatelets has been successfully calculated from the XRD data.[29] Here, we also calculated the size of Bi_2Te_3 nanowires from the XRD data. During the Rietveld refinements, besides the structural parameters, three shape parameters are refined and the anisotropic crystallite sizes are calculated from the peak shape parameters. The refined parameters and crystallographic details from the Rietveld analysis are listed in **Table 1**. The refinements of the XRD data show that Bi_2Te_3 nanowires have crystallite sizes of 20(1) and 17(1) nm along *a* and *c* directions, respectively. The identical crystallite sizes along *a* and *c* directions also suggest that the Bi_2Te_3 nanowires have different orientations. Thus, the crystallite size calculated by XRD is an average value from the different dimensions of the nanowires, which should be larger than the diameter of Bi_2Te_3 nanowires. However, the calculated crystallite sizes are only slightly larger than the diameters (about 15 nm) observed by TEM images, which can be ascribed to the large microstrains along the *c* direction of the bent Bi_2Te_3 nanowires.

Table 1 Refined parameters of the XRD data of Bi_2Te_3, Sb_2Te_3 and Bi_2Te_3-Sb_2Te_3 nanowires.

Sample	Bi_2Te_3	Sb_2Te_3	Bi_2Te_3-Sb_2Te_3[a]
Data points	3495	3495	3495
Reflections	58	56	113
R_I (%)	5.79	8.26	3.33
R_F (%)	4.25	8.04	3.06
a (Å)	4.387(1)	4.269(1)	4.386(1)
c (Å)	30.47(1)	30.45(1)	30.51(1)
Size (along *a*) (nm)	20(1)	70(1)	18(1)
Size (along *c*) (nm)	17(1)	45(1)	18(1)

[a]The parameters of the main phase of Bi_2Te_3 are listed in the table for the Bi_2Te_3-Sb_2Te_3 sample and the refined cell parameters 4.273(1) Å and c = 30.47(1) Å are obtained for the second phase Sb_2Te_3 with a weight fraction of 11(1)%.

The facile hydrothermal method may be an efficient way to fabricate other tellurides with one-dimensional nanostructure. As a proof of concept, experiments were also performed for the fabrication of Sb_2Te_3 nanowires. However, Sb ions are more difficult to be reduced by glucose under the acidic condition at 0.2 M HCl, and only Te is obtained at the reaction temperature of 180 °C. By enhancing the reaction temperature to 220 °C, it is possible to synthesize Sb_2Te_3, but with coexisting of Te impurities. It is possible to promote the reaction by further enhancing the reaction temperature, however, it reaches the limit of the operating temperature of conventional autoclaves. Clearly, the reduction reaction will be also promoted under alkaline solution because carboxylic acids are produced during the reduction reaction. Therefore, a two-step hydrothermal route was proposed for the synthesis of Sb_2Te_3 nanowires in the present study: Te nanowires were initially synthesized under acidic condition in 0.2 M HCl under a reaction temperature at 150 °C for 12 h, and Sb_2Te_3 nanowires were then fabricated by a second hydrothermal procedure under basic condition at a reaction temperature of 220 °C for 24 h. **Fig. 5(a)** is the XRD pattern and Rietveld refinement profile for Sb_2Te_3 prepared by the two-step hydrothermal route, indicating that single phase of Sb_2Te_3 was successfully obtained. The calculated unit cell parameters of Sb_2Te_3 nanowires are a = 4.269(1) Å and c = 30.45(1) Å. **Fig. 5(b)** and **(c)** are the typical SEM images in different magnifications showing that Sb_2Te_3 sample is composed of nanowires in high yield. It can be seen from the TEM image (**Fig. 5(d)**) that a layer of organic compound is coated on the surface of the Sb_2Te_3 nanowires. **Fig. 5(e)** is a HRTEM image showing a single-crystalline Sb_2Te_3 nanowire with the axis parallel to the c axis. The XRD results show that Sb_2Te_3 nanowires have crystallite sizes of 70(1) and 45(1) nm along a and c directions, respectively, which are much larger than the diameters of the nanowires observed by TEM images, indicating that the Sb_2Te_3 nanowires have different orientations. The calculated crystallite sizes by XRD are larger than those of Bi_2Te_3 nanowires, indicating that Sb_2Te_3 nanowires have a better crystallinity due to the enhanced reaction temperature and the different pH environment.

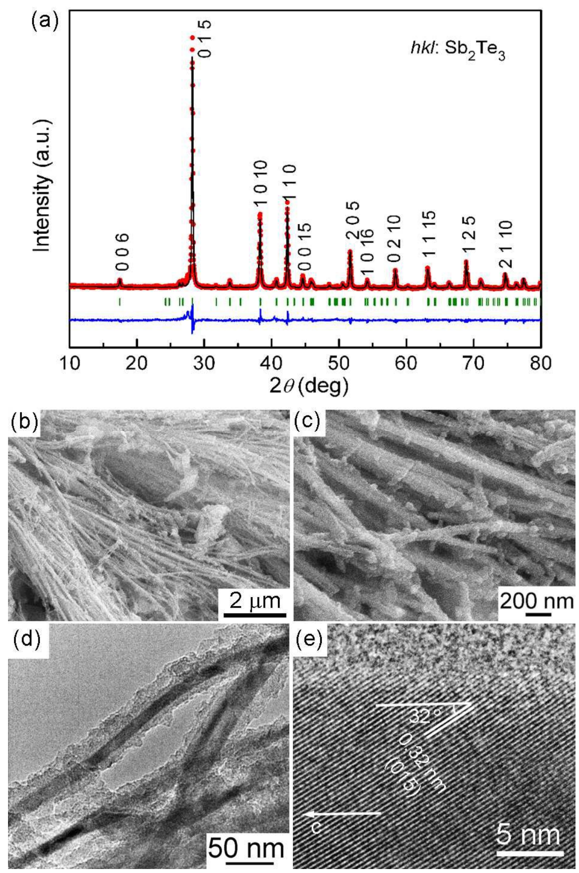

Fig. 5 (a) Observed, calculated and difference XRD patterns of Sb_2Te_3 sample prepared by two-step hydrothermal synthesis. (b,c) SEM images of the as-prepared Sb_2Te_3 nanowires. (d,e) TEM and HRTEM images of Sb_2Te_3 nanowires.

In view of searching better thermoelectric materials, ternary compounds such as $Bi_xSb_{2-x}Te_3$ ($0<x<2$) should be considered. Despite of many studies on chemical synthesis of Bi_2Te_3 based compounds, the knowledge about the alloying effects under solution synthesis of Bi_2Te_3 based ternary compounds is limited. Herein, Bi_2Te_3-Sb_2Te_3 nanowires were also prepared by the two-step hydrothermal method. **Fig. 6(a)** is the XRD pattern and Rietveld refinement profile for Bi_2Te_3-Sb_2Te_3 product. It can be seen both Bi_2Te_3 and Sb_2Te_3 phases are present in the product. The calculated cell parameters are 4.386(1) Å and c = 30.51(1) Å for Bi_2Te_3, and 4.273(1) Å and c =

30.47(1) Å for Sb_2Te_3, respectively. The weight fractions are 89(1)% and 11(1)% for Bi_2Te_3 and Sb_2Te_3, respectively, calculated from the XRD data. It can be suggested that part of the Sb atoms are alloyed in Bi_2Te_3. **Fig. 6(b)** and **(c)** show the typical SEM images of the as prepared Bi_2Te_3-Sb_2Te_3 products confirming the formation of one-dimensional nanostructures. The TEM image (**Fig. 6(d)**) shows that the Bi_2Te_3-Sb_2Te_3 nanowires have the diameters about 25 nm with a thick layer of organic compounds coated on the surface. Unlike single-crystalline Bi_2Te_3 nanowires and Sb_2Te_3 nanowires, the HRTEM image (**Fig. 6**) of Bi_2Te_3-Sb_2Te_3 nanowires shows different sets of lattice planes along varied orientations. HRTEM image (**Fig. S6**) of another Bi_2Te_3-Sb_2Te_3 sample shows structural fluctuation in the nanowires. Lattice mismatch is found by the fast Fourier transform (FFT) of the lattice-resolved image. The structure fluctuation in the Bi_2Te_3-Sb_2Te_3 nanowires may further adjust the band structure and increase the phonon scattering thus to optimize thermoelectric properties.

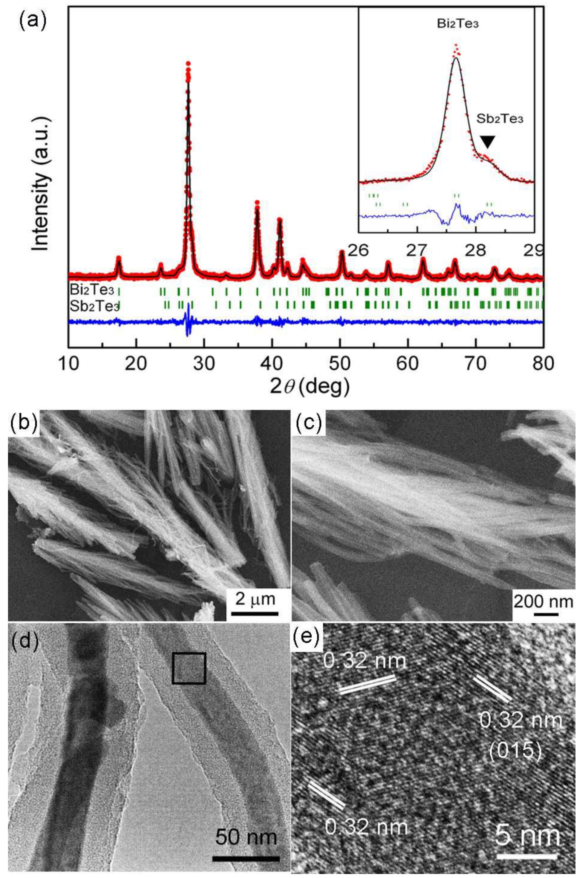

Fig. 6 (a) Observed, calculated and difference XRD patterns of Bi_2Te_3-Sb_2Te_3 sample prepared by two-step hydrothermal synthesis showing mixture of Bi_2Te_3 and Sb_2Te_3. (b,c) SEM images of the as-prepared Bi_2Te_3-Sb_2Te_3 nanowires. (d,e) TEM and HRTEM images of Bi_2Te_3-Sb_2Te_3 nanowires.

Fig. 7 shows the EDS elemental mapping analysis of the element distributions of Te, Sb and Bi, respectively, of the Bi_2Te_3-Sb_2Te_3 nanostructure. If we disregard the layer of organic compounds, it shows that the outmost layer of the crystalline nanowire mainly contains Sb and Te elements, indicating a possible formation of Sb-rich phase in the outer layer. As discussed before, it is difficult to form nanowires with a single phase of alloyed $BiSbTe_3$. For the formation of single phase of alloyed $BiSbTe_3$, it is assumed that the chemical properties of the cation ions (Bi and Sb ions in the present study) should be quite similar so they can be reduced and reacted with Te templates simultaneously. However, in the present study that Bi_2Te_3 is much easier to be formed than Sb_2Te_3, and the kinetic process of the formation of Bi_2Te_3 is faster than Sb_2Te_3 when the mild reducing agent of glucose is used during the hydrothermal synthesis. This is proved by the XRD patterns of the samples prepared at different reaction times (**Fig. S7**). As a result, it is possible that the formation Bi_2Te_3 should precede that of Sb_2Te_3, resulting the structure and composition fluctuation in the Bi_2Te_3-Sb_2Te_3 nanowires.

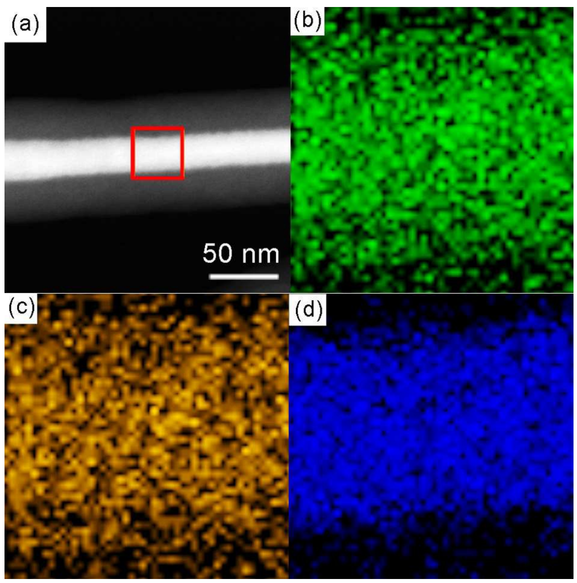

Fig. 7 (a) TEM image of a single Bi_2Te_3-Sb_2Te_3 nanowire. (b-d) EDS elemental mapping analysis of the element distributions of Te (b), Sb (c) and Bi (d) for the selected area in (a), indicating a composition fluctuation in Bi_2Te_3-Sb_2Te_3 nanowires.

Conclusion

A facile and scalable glucose-assisted hydrothermal method is demonstrated for the fabrication of Bi_2Te_3, Sb_2Te_3 and Bi_2Te_3-Sb_2Te_3 with one-dimensional nanostructures. Bi_2Te_3 nanowires with different orientations are obtained by direct one-step hydrothermal synthesis under acidic condition, in which Te nanowires form first and they serve as templates for the fabrication of Bi_2Te_3 nanowires. Structural preference growth mechanism and coherent growth mechanism are suggested for the formation of Bi_2Te_3 nanowires. A two-step hydrothermal synthesis is proposed for the fabrication of Sb_2Te_3 and Bi_2Te_3-Sb_2Te_3 nanowires by varying the pH conditions at different steps. Bi_2Te_3-Sb_2Te_3 heterostructure nanowires may provide a potential way for adjusting the band structure and for further improving the thermoelectric properties of low dimensional Bi_2Te_3 based materials.

Acknowledgements

The work was supported by the National Natural Science Foundation of China (Grant No. 51401089), the Natural Science Foundation of Jiangsu Province (Grant No. BK20140552, Grant No. BK20140013), the Scientific Research Foundation of Jiangsu University (Grant No. 14JDG013, Grant No. 11JDG098).

References

1 G. J. Snyder and E. S. Toberer, *Nat. Mater.*, 2008, **7,** 105-114.

2 J. P. Heremans, V. Jovovic, E. S. Toberer, A. Saramat, K. Kurosaki, A. Charoenphakdee, S. Yamanaka and G. J. Snyder, *Science*, 2008, **321,** 554-557.

3 Y. Pei, H. Wang and G. J. Snyder, *Adv. Mater.*, 2012, **24,** 6125-6135.

4 M. S. Dresselhaus, G. Chen, M. Y. Tang, R. Yang, H. Lee, D. Wang, Z. Ren, J. P. Fleurial and P. Gogna, *Adv. Mater.*, 2007, **19,** 1043-1053.

5 T. C. Harman, P. J. Taylor, M. P. Walsh and B. E. LaForge, *Science*, 2002, **297,** 2229-2232.

6 R. Venkatasubramanian, E. Siivola, T. Colpitts and B. O'Quinn, *Nature*, 2001, **413,** 597-602.

7 A. I. Boukai, Y. Bunimovich, J. Tahir-Kheli, J. K. Yu, W. A. Goddard III and J. R. Heath, *Nature*, 2008, **451,** 168-171.

8 A. I. Hochbaum, R. Chen, R. D. Delgado, W. Liang, E. C. Garnett, M. Najarian, A. Majumdar and P. Yang, *Nature*, 2008, **451,** 163-167.

9 B. Poudel, Q. Hao, Y. Ma, Y. Lan, A. Minnich, B. Yu, X. Yan, D. Wang, A. Muto, D. Vashaee, X. Chen, J. Liu, M. S. Dresselhaus, G. Chen and Z. Ren, *Science*, 2008, **320,** 634-638.

10 K. F. Hsu, S. Loo, F. Guo, W. Chen, J. S. Dyck, C. Uher, T. Hogan, E. K. Polychroniadis and M. G. Kanatzidis, *Science*, 2004, **303,** 818-821.

11 A. I. Hochbaum and P. Yang, *Chem. Rev.*, 2010, **110,** 527-546.

12 L. D. Hicks and M. S. Dresselhaus, *Phys. Rev. B*, 1993, **47,** 16631-16634.

13 A. Mavrokefalos, A. L. Moore, M. T. Pettes, L. Shi, W. Wang and X. Li, *J. Appl. Phys.*, 2009, **105,** 104318.

14 B. Hamdou, J. Kimling, A. Dorn, E. Pippel, R. Rostek, P. Woias and K. Nielsch, *Adv. Mater.*, 2013, **25,** 239-244.

15 S. I. Kim, K. H. Lee, H. A. Mun, H. S. Kim, S. W. Hwang, J. W. Roh, D. J. Yang, W. H. Shin, X. S. Li, Y. H. Lee, G. J. Snyder and S. W. Kim, *Science*, 2015, **348,** 109-114.

16 N. Han, S. I. Kim, J. D. Yang, K. Lee, H. Sohn, H. M. So, C. W. Ahn and K. H. Yoo, *Adv. Mater.*, 2011, **23,** 1871-1875.

17 H. Zhang, C. X. Liu, X. L. Qi, X. Dai, Z. Fang and S. C. Zhang, *Nat. Phys.*, 2009, **5,** 438-442.

18 J. Song, F. Xia, M. Zhao, Y. L. Zhong, W. Li, K. P. Loh, R. A. Caruso and Q. Bao, *Chem. Mater.*, 2015, **27,** 3471-3482.

19 W. Wang, B. Poudel, J. Yang, D. Z. Wang and Z. F. Ren, *J. Am. Chem. Soc.*, 2005, **127,** 13792-13793.

20 Y. Zhang, L. P. Hu, T. J. Zhu, J. Xie and X. B. Zhao, *Cryst. Growth Des.*, 2013, **13,** 645-651.

21 A. L. Prieto, M. S. Sander, M. S. Martín-González, R. Gronsky, T. Sands and A. M. Stacy, *J. Am. Chem. Soc.* 2001, **123,** 7160-7161.

22 C. L. Chen, Y. Y. Chen, S. J. Lin, J. C. Ho, P. C. Lee, C. D. Chen and R. Harutyunyan, *J. Phys. Chem. C* 2010, **114,** 3385-3389.

23 M. S. Sander, A. L. Prieto, R. Gronsky, T. Sands and A. M. Stacy, *Adv. Mater.*, 2002, **14,** 665−667.

24 M. S. Sander, R. Gronsky, T. Sands and A. M. Stacy, *Chem. Mater.*, 2003, **15,** 335−339.

25 J. L. Mi, N. Lock, T. Sun, M. Christensen, M. Søndergaard, P. Hald, H. H. Hng, Y. Ma and B. B. Iversen, *ACS Nano*, 2010, **4,** 2523-2530.

26 Z. H. Ge and G. S. Nolas, *Cryst. Growth Des.*, 2014, **14,** 533-536.

27 J. Rodriguez-Carvajal, *Physica B*, 1993, **192,** 55-69.

28 Y. Feutelais, B. Legendre, N. Rodier and V. Agafonov, *Mater. Res. Bullet.* 1993, **28,** 591−596.

29 J. L. Mi, M. Christensen, C. Tyrsted, K. Ø. Jensen, J. Becker, P. Hald and B. B. Iversen, *J. Phys, Chem. C*, 2010, **114,** 12133-12138.

30 H. T. Zhu, J. Luo, H. M. Fan, H. Zhang, J. K. Liang, G. H. Rao, J. B. Li, G. Y. Liu and Z. M. Du, *J. Mater. Chem.*, 2011, **21,** 12375-12380.

31 W. Ning, H. Du, F. Kong, J. Yang, Y. Han, M. Tian and Y. Zhang, Y., *Sci. Rep.*, 2013, **3,** 1564.

32 J. Kang, J. S. Noh and W. Lee, *Nanoscale Res. Lett.*, 2011, **6,** 277.

Graphical Table of Contents

A facile and "green" glucose-assisted hydrothermal method is proposed to synthesize Bi_2Te_3, Sb_2Te_3 and Bi_2Te_3-Sb_2Te_3 nanowires.